Granular Dynamics of a Vibrated Bed of Dumbbells

R. D. Wildman[1], J. Beecham[2], and T. L. Freeman[2]

[1] School of Mechanical and Manufacturing Engineering, Loughborough University,
   Loughborough Leics. LE11 3TU, United Kingdom
[2] School of Computer Science, University of Manchester, Manchester M13 9PL, United Kingdom

Abstract. A two-dimensional vibrated bed of dumbbells was investigated using experiment and numerical simulation. Experimentally, high speed photography in combination with image analysis and tracking software was used to determine the location of the centre of mass and the locations and direction of motion of the component particles of the dumbbells. Numerically, a geometry analogous to that used experimentally was employed and the equations of motion for each of the particles were solved using the distinct element method. It was found that, despite some differences, the numerical simulations agreed reasonably well with the experimental results. Subsequently, the simulation method was used to explore the behaviour of the bed over a range of densities. The moments of the velocity distributions were determined as a function of height for a range of numbers of particles, and it was found that a normal distribution of velocities is a good approximation, except close to the vibrating base where there were suggestions that the distribution of the vertical component of the velocities is a composite of two sets of particles, one pre-collision with the base, and the other post-collision.

1 Introduction

Over the last few decades a large number of experiments have been performed to study the behaviour of granular materials under a range of flow conditions. On the whole, this has been motivated by the need to understand the complex phenomena that arise during particle flow. For example, experiments have demonstrated the presence of buoyancy induced convection [1], clustering [2], pattern formation [3,4] and segregation [5]. Many researchers have depended on a continuum or hydrodynamic approach to describe these results, with arguably the most successful route to building such a description being the kinetic theory method. This builds on the development of the gas kinetic theory of Maxwell, Boltzmann, and Chapman and Enskog, resulting in the prediction of the constitutive relations required for closure of the equations that govern the balance of mass, heat and energy (see [6,7] for examples of these for granular media). This approach, modified to be applicable to dissipative systems, was initially confined to smooth, nearly elastic hard disk or spherical particles [6,8]. Subsequently, however, the methodology was extended to rough particles [9,10] and more recently to systems of particles that may take any coefficient of restitution from 0 to 1 [11]. Including the roughness implicitly acknowledges that the spin of the particles, and the manner in which the translational and rotation motion is coupled, can have a significant influence on the behaviour of a bed of particles and this has led to modified versions of the constitutive relations that include the contribution of the rotational granular temperature to the source of translational energy and flux of rotational energy. However, these contributions relate to spherical particles interacting through friction and though they develop the concept of spin granular temperature, they do not provide insight into the coupling of translation and rotational motion by mechanisms relating to shape rather than friction.

A key difference between molecular gas systems and fluidised granular systems is that granular particles lose energy during collisions, which has a number of consequences. These include granular systems being unable to exist in an equilibrium state and behaviour and properties being direction dependent. This anisotropy is often observed, but rarely considered theoretically, despite the differences between the energy in each direction being as large as 50% [12,13]. The principal reason for this apparent lack of interest is that one must go beyond the Navier-Stokes level of continuum approximation and start to consider Burnett and super-Burnett corrections. This means that equipartition of energy cannot be assumed; indeed it is unlikely to be present, as has been observed in a number of experiments and predicted analytically (for anisotropy in granular flows see for example, [7,14–16]), in polydisperse flows [15,17–21] and anticipating the results of this paper, we would not expect to see equipartition between rotational and translational modes.

A number of researchers have begun to consider the effect of particle anisotropy on bulk behaviour. Huthmann et al [22] made the first study of the homogenous cooling state of a gas of rods. They observed that the system quickly decayed to a fixed ratio of translational temperature to rotational temperature. Importantly they found that in general equipartition was not observed, except for special cases of mass distribution along the needles. Building on this work, Viot and Talbot [23] were able to show analytically that the granular temperatures associated with translation and the rotation of needles are different. An extension of this study has led to the development of a Boltzmann equation for a discorectangle, providing the basis of an analysis of a non-equilibrium steady state consisting of a bath of particles and an anisotropic intruder particle [24]. Again, they found that the translational granular temperature was consistently higher than the rotational, except when the coefficient of restitution was varied as a function of position. These studies have highlighted the complexity of constructing and solving collision integrals for aspherical particles and demonstrate how far we are from having constitutive relations that will enable us to predict the behaviour of flows with non-spherical shape and complex morphology. Compounding this are the very few experimental studies that have considered the effect of anisotropy (see for example the study of the motion of linked spheres on a horizontal plate by Atwell and Olafsen [25] or the recent study of the dynamics of a single bouncing dimer [26]), an aspect of this field we aim to address with this paper.

In this paper we propose to measure the key characteristics of a simple granular flow of anisoptropic particles. We consider dumbbells, essentially two spheres or disks fused together, as a starting point for investigating the effect of shape on the behaviour of a granular bed. The study is split into two parts. Firstly we will perform experiments on a two-dimensional vibrated bed of dumbbells and compare the results to distinct element simulations. In the case of the experimental study we use high speed photography and appropriate post-processing to observe the motion of the dumbbells and determine the velocity distributions, the density profile and the granular temperature as a function of height. Secondly, we use the simulations to extend the investigation to consider the behaviour of the moments of the velocity distribution as a function of height in the bed.

2 Experiment and Simulation

We will first introduce the experimental technique employed to generate a two-dimensional gas of dumbbells, and then describe the method used to obtain the coordinates of the particles. We will then discuss the numerical simulation and the parameters used. Subsequent sections will discuss the results of the experiment and the simulations together.

2.1 Experimental Method

2.1.1 Apparatus

A two-dimensional plane of motion was created by constructing a cell, 145 mm in width, 200 mm high, consisting of two parallel glass plates that act to constrain beads placed between

them into two degrees of translational freedom. The plates were positioned 5.05 mm apart minimising the particle-wall friction energy losses [27]. The cell was moved using an electro-magnetic transducer (LDS V651) vibrating at a frequency of 50 Hz and an amplitude of 0.85 mm. A signal generator generates a sinusoidal waveform, which was passed through a power amplifier and drives the platform upon which the cell sits. The dumbbells were constructed from glass ballotini beads, diameter, σ, of 5 mm, which were attached in pairs with glass glue, creating a dumbbell with a bond length l, of 5 mm, or one bead diameter. The restitution coefficient between individual glass beads was measured using high-speed photography and found to be $\varepsilon = 0.91$. Two experiments were performed, first with just under one layer of dumbbells (number of particles, $N = 14$), and secondly with two layers of dumbbells ($N = 29$), where N is the total number of dumbbells in the system.

2.1.2 High Speed Photography

The particle motion was captured using a high-speed high resolution CCD camera (Vosskuhler 1000). The cell was illuminated from behind and the light was focussed onto the CCD array of the digital camera. This resulted in a set of black particles on a white background. Following a capture sequence the images were uploaded to a PC for storage and processing. During the analysis phase, each frame was examined to determine the centres of the particles. We employed a Hough Transform based technique to locate the centres of all the spheres in the field of view [27,28]. This technique is particularly robust, and allows the determination of the centre of the particle even when the whole particle is not visible. In our case, this is an extremely useful property of the technique, as the bond between the two particles forming the dumbbell obscures a portion of the edge of each grain and the Hough Transform has proved a reliable way of determining the location of spherical grains not wholly in the field of view.

2.1.3 Particle Tracking

The next step is to associate each grain with a "partner", i.e., connect two grains together into a dumbbell, and then track the motion of the dumbbell through each frame. We do this by first tracking all the particles through all the images, determining their coordinates using the Hough Transform technique [27]. We then look for grains that are always at a fixed distance, σ, from each other. Though some grains will pass close to each other during the vibration, or even collide with each other, only one pair will always be found at a fixed separation. These two particles are confined to move a fixed distance apart, and we label them as being part of the same dumbbell. Having selected pairs of grains to be considered as single entities, we assign a label in order to track their motion and to determine the x and y coordinates of the centre of mass of the dumbbell and its orientation.

2.2 Numerical Simulations

Numerical simulations of the particle motion provide insight into a range of behaviour that is not readily accessible to experiment. One can track all of the particles and determine their positions, velocities and accelerations throughout the whole of the domain for extended periods of time at machine accuracy. A number of techniques are available, including Monte Carlo simulations [29,30] and hard sphere or event driven simulations [31], but here we choose to employ the Distinct Element Method (DEM) (see, for example, the review of contact models used in DEM by Stevens and Hrenya [32]). This method solves the equations of motion for both ballistic flight and during collisions and provides considerable flexibility in the choice of collision model [32].

In our case the simulation geometry consisted of elastic side boundaries, an elastic top and a vibrating dissipative boundary at the base. The simulated dumbbells were created from a pair of disks (diameter, σ) linked together with a fixed separation of one particle diameter. The

particles were subjected to an external force, in this case equal to gravity. When the distance between a disc centre and a neighbouring disc centre was found to be less than a sphere diameter, the contact force, F, was given by a Hertzian-like interaction law with dissipation proportional to the relative velocities, v, of the centres of the component particles in contact [32]. The law is given by

$$F = -kx^{3/2} - bv \tag{1}$$

where x is the overlap of the particles,

$$x = |r - \sigma| \ , \tag{2}$$

and where r is the distance between the centres of the colliding component disks, k is an effective spring constant and b is the particle-particle dissipation parameter. There are a number of variants on the force law, all producing different behaviour, particularly in the variation of restitution coefficient with velocity (see for example, [32–34]). We use this law since it behaves relatively well at high velocities, though discrepancies with experiment are noted at low speed impacts. The interaction with the walls was assumed to be elastic, and given by a Hookian law,

$$F_w = -k_w x \tag{3}$$

where F_w is the contact force between the wall and a particle and in this case x represents the overlap of the particle and the wall.

At every time step the forces on each particle (i.e., gravitational and collisional) are summed, and the acceleration, velocity and position are updated accordingly. The simulation then proceeds to step forward in time and repeats the process of force determination and position updating.

The use of a spring and dissipation mechanism for controlling energy dissipation during collisions means that a coefficient of restitution close to that observed in experiment cannot be specified easily. To overcome this problem, we first solved the differential equation specified by introducing the acceleration into Eq. 1, and calculated the Newtonian coefficient of restitution. This served as an initial estimate of the coefficient of restitution. The spring constant and the dissipation coefficient were then changed in an iterative fashion to provide a good match between the numerically and the experimentally determined density profiles whilst ensuring that the time of collision was much longer than the chosen time step. We used a combination of k and b that meant that the particles were somewhat "softer" than real particles, but this allowed for a combination of time step and time of collision such that simulations could be completed within a reasonable timeframe ($k = 40$ kg/(m$^{1/2}$s), $b = 0.01$ kg/s and $k_w = 40$ kg/s^2). This resulted in contact durations that ranged from 34 ms to 6 ms for impact velocities of 0.1 m/s and 3.0 m/s respectively.

The simulations were run for typically 1.5 s of simulated time to allow for steady state to be reached, which was checked by examining the energy in the system as a function of time. After the steady state was achieved, the simulations were run for up to a further 15 s. One drawback of using soft particles, however, was that on rare occasions the particles had sufficient relative velocity that the dumbbells could overlap and become fixed into a stable quadrapole geometry. To avoid this occurrence we included a steep short range potential between the centres of masses of the dumbbells causing strong repulsion as they approached each other closely. A snapshot of the configuration of the dumbbells for $N = 29$ is shown in Fig. 1.

3 Measurement of key variables

The behaviour of the granular bed can be characterised through a number of key variables. Particularly important are the velocity distributions, from which many features such as the mean velocity and granular temperature can be deduced. In addition the velocity distributions serve as a basis for deriving constitutive equations in theoretical models. We will use the moments of the velocity distribution to calculate the following quantities as a function of height: the
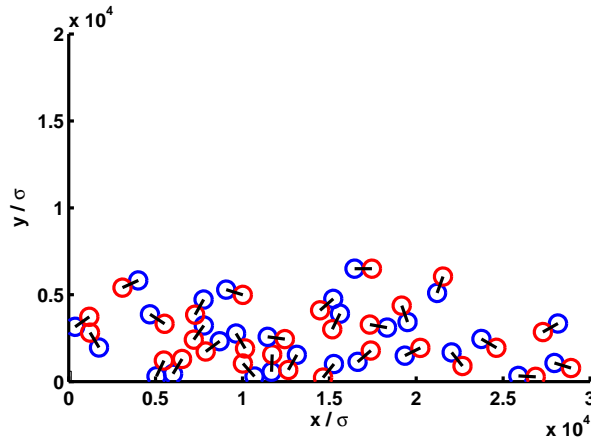
Fig. 1. A snapshot of a numerical simulation of a 2D vibrated bed consisting of $N = 29$ particles, after the system had reached the steady state.

mean velocity and the granular temperature from the first two moments, and the heat flux and measures of non-Gaussian behaviour from the third and fourth moments respectively. We use both the experimental and numerical data to compare the granular temperature and packing fraction, whilst the numerical simulations allow the velocity distribution and moments to be examined in detail.

3.1 Granular Temperature

Figures 2 and 3 show the granular temperature profiles as a function of height for 1 and 2
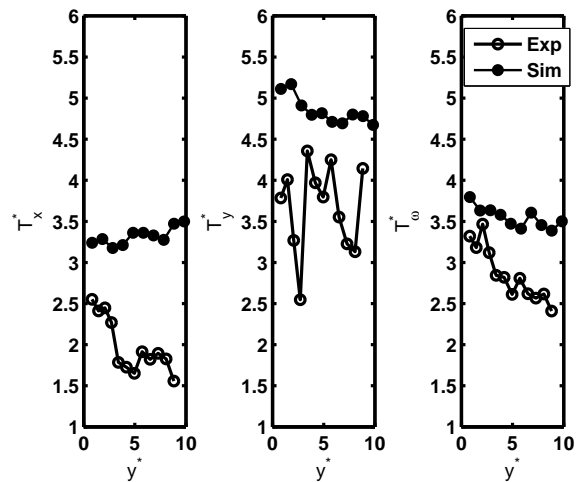

Fig. 2. A comparison of the granular temperature calculated from experimental and numerical simulation data as a function of height for $N = 14$.

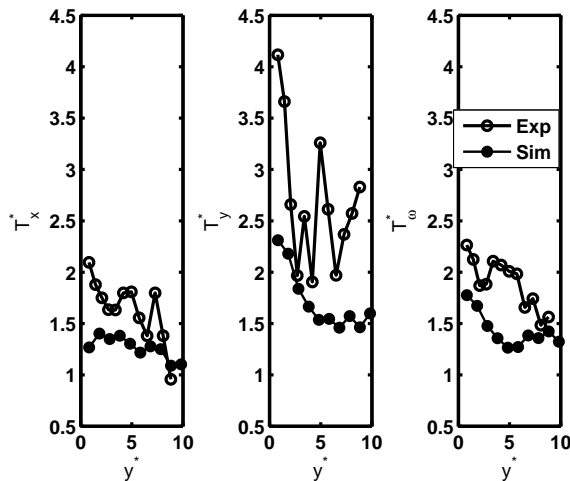layers of beads respectively, for both the simulation and the experimental data. We define the

Fig. 3. A comparison of the granular temperature calculated from experimental and numerical simulation data as a function of height for $N = 29$.

granular temperature, T, as

$$T_i = m\overline{(v_i - \overline{v_i})^2} \tag{4}$$

and

$$T_\omega = I\overline{(\omega - \overline{\omega})} \tag{5}$$

where I is the moment of inertia. For the case where the separation between the centre of the component particles is equal to the diameter of a component particle ($l = \sigma$) the moment of inertia for a dumbbell is given by

$$I = \frac{14}{40}m\sigma^2 \,. \tag{6}$$

The granular temperatures are non-dimensionalised by $mg\sigma$ and the height by σ. In previous studies of granular beds, it has been possible to observe two degrees of freedom (or three in three-dimensional studies), i.e., the motion in the horizontal and vertical directions. However, here we also see the behaviour of the rotational mode. As is usual for a system such as this [13], the y granular temperature is significantly higher than the granular temperature associated with the x direction. In addition we see that experimentally, the rotational component of the granular temperature has a magnitude that lies between that of the y and the x components. One should of course anticipate that the spin granular temperature is higher than the x component, as the base not only acts as a source of y granular temperature, but also of spin granular temperature. However, as the post-collisional angular velocity is strongly dependent on the angle of impact, the flux of energy into the rotational modes will not necessarily be expected to be as large as that into the y translational motion. One also sees, in all three temperatures, a trend of reduced granular temperature with height, as one would expect due to the loss of kinetic energy during collisions. When we compare Fig. 2 and 3 we observe that in the former case that the experimental temperatures are lower than those in the simulation, but in the latter this relationship is inverted. One possible cause of this is the dependence of the contact mechanics on the relative velocities has not been correctly captured, suggesting that further work should focus on the particle-particle interactions in more detail.

3.2 Packing fraction

The packing fraction is calculated by summing the cross-sectional area of particles in the field of view and then dividing by the area of the field of view. Figures 4 and 5 show the packing
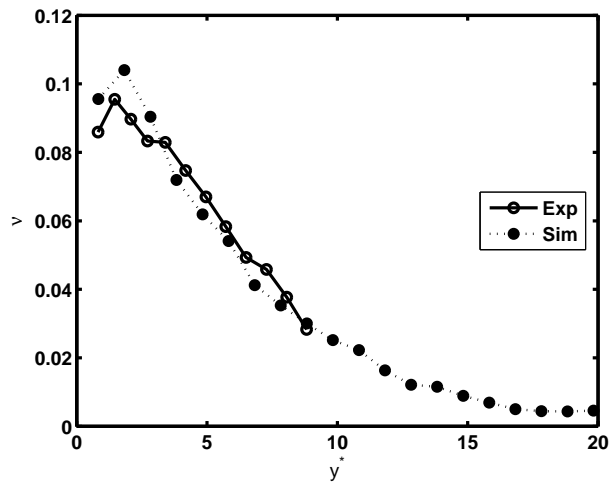
Fig. 4. A comparison of the packing fraction calculated from experimental and numerical simulation data as a function of height for $N = 14$.
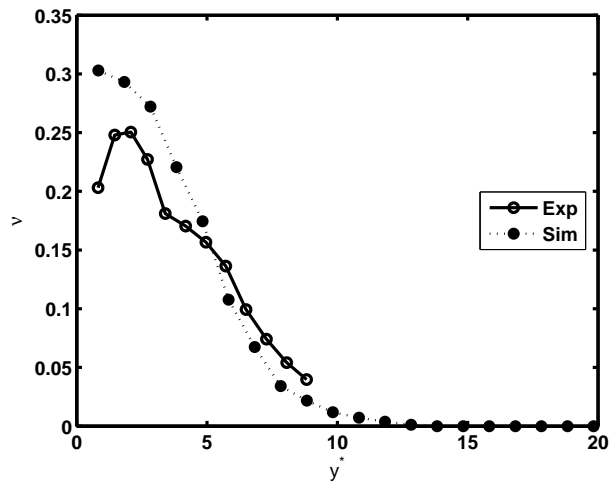

Fig. 5. A comparison of the packing fraction calculated from experimental and numerical simulation data as a function of height for $N = 29$.

fraction profiles for one and two layers of beads. These profiles are reminiscent of those for spherical beads: the packing fraction profile is "humped". However, the profile at the base is more complex because of the orientation of the dumbbells; the distance between the base and the dumbbell centre of mass depends upon the orientation of the dumbbells. At higher altitudes the packing fraction reduces asymptotically to zero.

3.3 Velocity distributions

Experimentally, in order to reliably measure the velocity distributions of the particles, we are required to determine the velocities *between* collisions. In order to achieve this, we detected collisions by determining the periods during which centres of the spherical component particles were in close proximity ($\sim 1.1\sigma$) with another particle, and then separated the dumbbell tracks into short trajectories of free motion. The velocities in the x (horizontal), the y (vertical)

directions and also the angular velocity, were determined by performing least square regression on the dumbbell tracks and orientation as a function of time, first order in the case of the x and θ coordinates, and second order in the case of the y coordinate. The dumbbell velocity at each time step was then extracted. In the case of the θ coordinate, before extracting the angular velocity a further step of "unwrapping" was required to account for the wrapping of the angle of orientation onto the range 0 to 2π radians.

The extracted velocities were then sorted into disjoint bins and a velocity distribution for each coordinate constructed. A common assumption for granular flows is that the velocity distribution is Gaussian, but studies have shown that this is not necessarily a good description. To examine the distributions more closely, we compare the measured probability distributions, $P[v_i]$ and $P[\omega]$, against Gaussian distributions with the same 2nd moment, i.e., using distributions given by

$$P[v_i] = \frac{1}{\left(2\pi\overline{(v_i - \overline{v_i})^2}\right)^{1/2}} \exp\left(-\frac{v_i^2}{2\overline{(v_i - \overline{v_i})^2}}\right) \tag{7}$$

and

$$P[\omega] = \frac{1}{\left(2\pi\overline{(\omega - \overline{\omega})^2}\right)^{1/2}} \exp\left(-\frac{\omega^2}{2\overline{(\omega - \overline{\omega})^2}}\right) \tag{8}$$

where the subscript i denotes the x or y direction, v_i is the linear velocity of the centre of mass of the dumbbell, ω is the angular velocity of the dumbbell and $\overline{v_i}$ and $\overline{\omega}$ are the mean linear velocity and mean angular velocity respectively. This was done for both the experimental and numerical simulation velocity distribution profiles. The granular temperature is a measure of the energy of the fluctuations about the mean velocity.

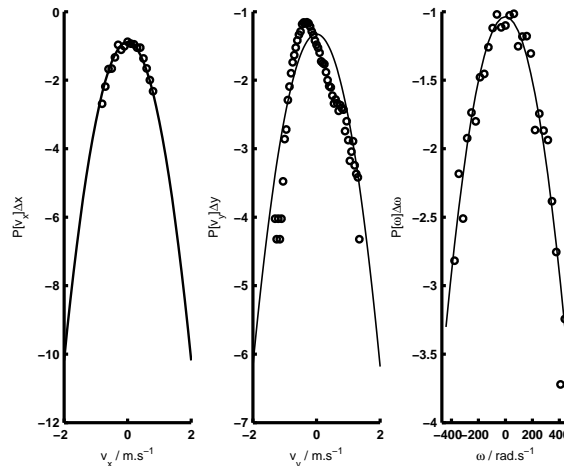Figures 6 and 7 show the experimentally determined velocity distributions on log-normal

Fig. 6. Velocity distributions on log-normal axes for (a) x, (b) y and (c) θ directions, for a system containing $N = 14$ particles in the height range, $y = 0$ to 2σ. The symbols show the experimental results with the solid line showing a normal distribution.

axes for $N = 14$ and $N = 29$, for the range $y = 0$ to 2σ. These figures show strong asymmetry in the vertical direction, though it's less marked for the system with greater numbers of particles. Importantly, we also see that the behaviour in the horizontal and rotational directions is Gaussian. Figures 8 and 9 show the velocity distributions obtained from numerical simulation for $N = 14$ in the height interval, 0 to σ, and from 3σ to 4σ. The y-velocity distribution shows
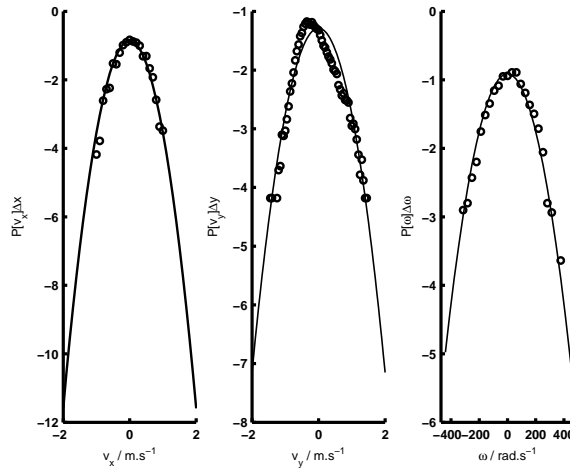
Fig. 7. Velocity distributions on log-normal axes for (a) x, (b) y and (c) θ directions, for a system containing $N = 29$ particles in the height range, $y = 0$ to 2σ. The symbols show the experimental results with the solid line showing a normal distribution with the same second moment.
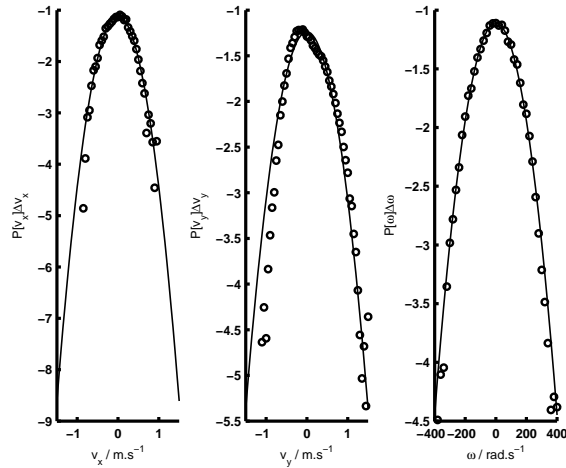

Fig. 8. Velocity distributions on log-normal axes for (a) x, (b) y and (c) θ directions, for a system containing $N = 14$ particles in the height range, $y = 0$ to σ. The symbols show the numerical simulation results with the solid line showing a normal distribution with the same second moment.

strong asymmetry, near to the base, but becomes Gaussian at a few particle diameters. This can be associated with a non-zero third moment of the distribution and the transfer of granular "heat" upwards from the base. Interestingly we see some evidence of the behaviour predicted by Ramírez and Cordero [35], where the "shoulder" evident in the velocity distribution hints at particles moving in a viscous medium as they pass through the surrounding gas of particles.

A related way of considering this behaviour is to view the particle cloud as being composed of two sets of grains, one having recently encountered the base and one set yet to collide with it. The probability distributions for these sets of particles will be different, with notably different granular temperatures and different mean velocities. This composite distribution is not likely to be Gaussian, particularly if the first and second moments are substantially different in each cloud. Based on the idea that the distribution may have a contribution from two distinct
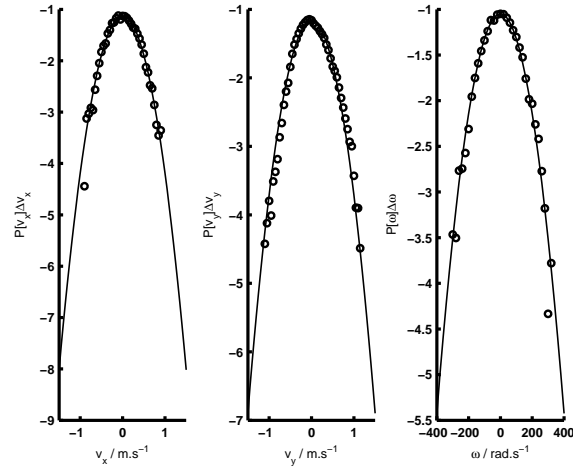
Fig. 9. Velocity distributions on log-normal axes for (a) x, (b) y and (c) θ directions, for a system containing $N = 14$ particles in the height range, $y = 3\sigma$ to 4σ. The symbols show the numerical simulation with the solid line showing a normal distribution with the same second moment.

populations, we can assume that the velocity distribution is of the form

$$
P\left[v_i\right] = a_1 \frac{m^{1/2}}{\left(2\pi T_{\text{pre}}\right)^{1/2}} \exp\left(-\frac{m\left(v_y - \overline{v_{y,\text{pre}}}\right)^2}{2T_{\text{pre}}}\right) + a_2 \frac{m}{\left(2\pi T_{\text{post}}\right)^{1/2}} \exp\left(-\frac{m\left(v_y - \overline{v_{y,\text{post}}}\right)^2}{2T_{\text{post}}}\right)
$$
(9)

where a_1 and a_2 are the fraction of particles in the pre- and post-collisional grain clouds respectively. The subscripts pre and post refer to the pre- and post-collisional granular populations. Using a non-linear regression algorithm we fitted this form of the distribution to that obtained from the numerical simulations. As can be seen from Figs. 10 and 11, the fitting is rather good.
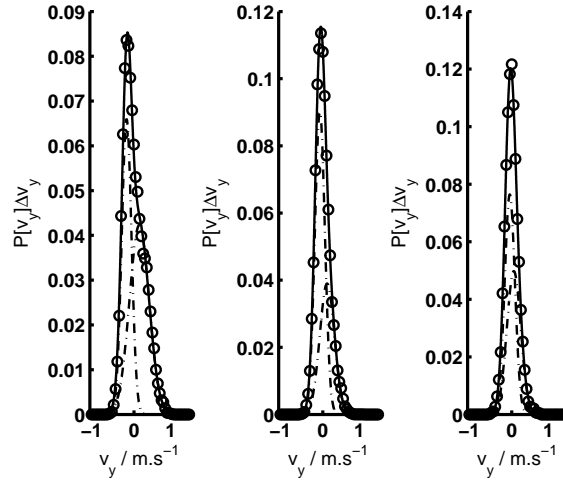

Fig. 10. A comparison of the velocity distribution obtained from numerical simulation and a fitted two population velocity probability distribution function for the height ranges $y = 0$ to σ, 2σ to 4σ and 4σ to 5σ, for $N = 14$.
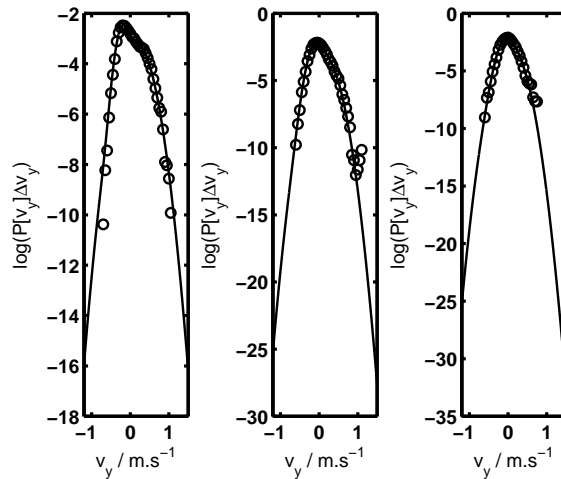
Fig. 11. A comparison of the velocity distribution obtained from numerical simulation and a fitted two population velocity probability distribution function on log-normal axes for the height ranges $y = 0$ to σ, 2σ to 4σ and 4σ to 5σ, for $N = 14$.

Near to the base the distributions are separated, but the mean velocity values converge towards zero and the "mixing" of the two populations is seen as we look at the distribution at higher altitudes.

3.4 Moments

The moments of the velocity distribution greater than the first were calculated in the following way

$$\langle v_i^n \rangle = \int_{-\infty}^{\infty} (v_i - \overline{v_i})^n \, P(v_i) \, dv_i \quad \text{for} \quad n > 1 \tag{10}$$

where n is the degree of the moment. The first moment is equivalent to the mean velocity and the granular heat flux is proportional to the third moment [6]. The "excess of kurtosis", is a measure of the departure from Gaussian behaviour and is given by

$$k_c = \frac{\langle v_i^4 \rangle}{\langle v_i^2 \rangle^2} - 3 \tag{11}$$

which is zero for a Gaussian distribution. The first moment and the excess of kurtosis for $N = 14$ are shown in Fig. 12. The components of the third moment are shown in Fig. 13. Since the behaviour is qualitatively similar, we don't show the moments for higher values of N. We don't show the second moment since this is equivalent to the granular temperature.

   We observe some clear trends in the moments. The first moment is generally close to zero, indicating that convection currents are small, particularly in relation to the size of the fluctuations about the mean velocity. The full third moment has nine components:

$$\begin{bmatrix} \langle v_x^3 \rangle & \langle v_y v_x^2 \rangle & \langle \omega v_x^2 \rangle \\ \langle v_x v_y^2 \rangle & \langle v_y^3 \rangle & \langle \omega v_y^2 \rangle \\ \langle v_x \omega^2 \rangle & \langle v_y \omega^2 \rangle & \langle \omega^3 \rangle \end{bmatrix}. \tag{12}$$

These are calculated as a function of the height, y, and are plotted in Fig. 13 for $N = 14$. We observe that of the 9 components, only those that relate the transfer of energy in the y-direction are non-zero, and typically $\langle v_y^3 \rangle$ and $\langle v_y \omega^2 \rangle$ are significantly larger than $\langle v_y v_x^2 \rangle$. The
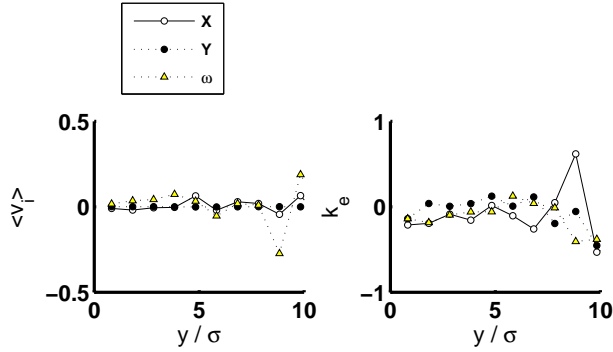
Fig. 12. Profiles of the first moment and excess of kurtosis of the velocity distribution as a function of height for $N = 14$.
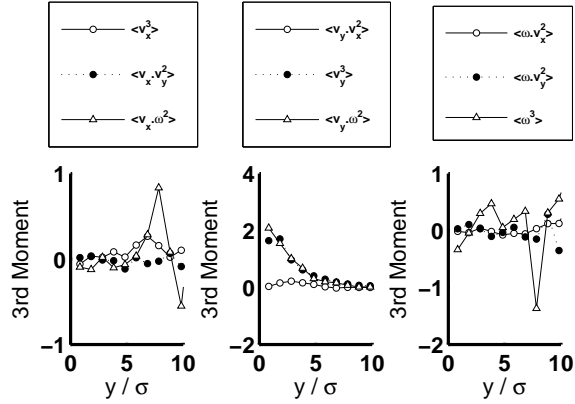

Fig. 13. Profiles of the components of the 3rd moment of the velocity distribution as a function of height for $N = 14$.

small magnitudes of the terms in columns 1 and 3 of (12) appear to reflect the symmetry in the velocity distributions and the small values of the gradients of the granular temperatures with respect to x and θ. However, to incorporate all such components of the third moment into a continuum description, and by implication the anisotropy, one is required to go beyond the Navier-Stokes level [36,37].

The excess of kurtosis provides an indication of whether the velocity distributions are close to Gaussian distribution. Figure 12b shows the excess of kurtosis for $N = 14$. We see some indications of non-Gaussian behaviour, particularly in the y direction, and to some extent in the angular velocity distribution. It is possible that the excess of kurtosis is caused by the heat flux, but as can be seen from a comparison of Figs. 12b and 13b the excess of kurtosis is consistently non-zero, even in the regions where the 3rd moment approaches zero. As we can see from Fig. 2, however, any deviations from a normal distribution are small. We do not observe any evidence for distributions with an exponent of ~ 1.5, which have been reported in a number of experimental and numerical simulations (see e.g. [38]). At larger numbers of particles we see

similar behaviour in the y direction; non-zero third moment and excess of kurtosis for the ω distribution.

4 Conclusion

It is clear from our results that, in general, anisotropic granular flows show similar behaviour to that of systems consisting of spherical particles. The transfer of energy in the vertical direction is mainly through the y component of velocity and the angular velocity modes which lead to interesting non-equilibrium behaviour.

The moments (and granular temperature) show significant anisotropy and reflect the transfer of kinetic energy, particularly close to the base. The complexity of the moments implies that a complete analysis of the full third moment will be necessary in order to describe the flow behaviour with kinetic theory. At the highest altitudes, however, we see close to Gaussian distributions, suggesting that descriptions of anisotropic granular behaviour that use near-Maxwellian distributions are likely to be successful.

Acknowledgements

References

1. R. D. Wildman, J. M. Huntley, D. J. Parker, Phys. Rev. Lett. **86**, 3304 (2001).
2. E. Falcon et al., Phys. Rev. Lett. **83**, 440 (1999).
3. P. B. Umbanhowar, F. Melo, H. L. Swinney, Nature **382**, 793 (1996).
4. C. Bizon, M. D. Shattuck, J. B. Swift, W. D. McCormick, H. L. Swinney, Phys. Rev. Lett. **80**, 57 (1998).
5. J. Baxter, U. Tuzun, D. Heyes, I. Hayati, P. Fredlund, Nature **391**, 136 (1998).
6. J. T. Jenkins, S. B. Savage, J. Fluid Mech. **130**, 187 (1983).
7. N. Sela, I. Goldhirsch, J. Fluid Mech. **361**, 41 (1998).
8. C. K. K. Lun, S. B. Savage, D. J. Jeffrey, N. Chepurniy, J. Fluid Mech. **140**, 223 (1984).
9. J. T. Jenkins, C. Zhang, Phys. Fluids **14**, 1228 (2002).
10. V. Kumaran, J. Fluid Mech. **561**, 1 (2006).
11. V. Garzo, J. W. Dufty, Physical Review E **59**, 5895 (1999).
12. H. Viswanathan, R. D. Wildman, J. M. Huntley, T. W. Martin, Phys. Fluids **18**, 113302 (2006).
13. R. D. Wildman, J. M. Huntley, D. J. Parker, Phys Rev E. **63**, 061311 (2001).
14. I. Goldhirsch, N. Sela, Phys Rev E. **54**, 4458 (1996).
15. R. D. Wildman, D. J. Parker, Phys. Rev. Lett. **88**, 064301 (2002).
16. J. Talbot, P. Viot, Phys. Rev. Lett. **89**, 064301 (2002).
17. V. Garzo, J. W. Dufty, C. M. Hrenya, Physical Review E **76**, 031303 (2007).
18. V. Garzo, C. M. Hrenya, J. W. Dufty, Physical Review E **76**, 031304 (2007).
19. R. D. Wildman, J. M. Huntley, Phys. Fluids **15**, 3090 (2003).
20. R. D. Wildman, J. T. Jenkins, P. E. Krouskop, J. Talbot, Phys. Fluids **18**, 073301 (2006).
21. S. R. Dahl, C. M. Hrenya, V. Garzo, J. W. Dufty, Physical Review E **66**, 041301 (2002).
22. M. Huthmann, T. Aspelmeier, A. Zippelius, Physical Review E **60**, 654 (1999).
23. P. Viot, J. Talbot, Physical Review E **69**, 051106 (2004).
24. H. Gomart, J. Talbot, P. Viot, Physical Review E **71**, 051306 (2005).
25. J. Atwell, J. S. Olafsen, Physical Review E **71**, 062301 (2005).
26. S. Dorbolo, D. Volfson, L. Tsimring, A. Kudrolli, Phys. Rev. Lett. **95**, 044101 (2005).
27. S. Warr, G. T. H. Jacques, J. M. Huntley, Powder Technol **81**, 41 (1994).
28. S. Warr, J. M. Huntley, G. T. H. Jacques, Phys Rev E. **52**, 5583 (1995).
29. M. A. Hopkins, H. H. Shen, J. Fluid Mech. **244**, 477 (1992).

30. J. J. Brey, M. J. Ruiz-Montero, Comput. Phys. Commun. **122**, 278 (1999).
31. S. McNamara, S. Luding, Phys Rev E. **58**, 813 (1998).
32. A. B. Stevens, C. M. Hrenya, Powder Technol. **154**, 99 (2005).
33. G. Kuwabara, K. Kono, Jpn. J. Appl. Phys. Part 1 - Regul. Pap. Short Notes Rev. Pap. **26**, 1230 (1987).
34. R. Ramírez, T. Pöschel, N. V. Brilliantov, T. Schwager, Physical Review E **60**, 4465 (1999).
35. R. Ramírez, D. Risso, R. Soto, P. Cordero, Phys Rev E. **62**, 2521 (2000).
36. J. T. Jenkins, M. W. Richman, J. Fluid Mech. **192**, 313 (1988).
37. N. Sela, I. Goldhirsch, J. Fluid Mech. **361**, 41 (1998).
38. J. S. van Zon, F. C. MacKintosh, Phys. Rev. Lett. **93**, 038001 (2004).